AUIQ Technical Engineering Science

Manuscript 1011

Biomechanical Insights of Head Trauma Based on Computational Simulation

Ghaidaa Abdulrahman Khalid

AUIQ TECHNICAL ENGINEERING SCIENCE 2024;1:22–30

ORIGINAL STUDY

Biomechanical Insights of Head Trauma Based on Computational Simulation

Ghaidaa Abdulrahman Khalid

Medical Instrumentaition Engineeering, Middle Technical University, College of Electrical and Electronic Engineering Techniques, 531653, Iraq

ABSTRACT

Head injuries from falls are a major cause of illness and death in children due to trauma. Despite their prevalence and impact, there is limited understanding of how children's heads react during impact events. Infant Post-Mortem-Human-Surrogate (PMHS) testing, a reasonable method for studying impact biomechanics, faces significant restrictions due to emotional, moral, and ethical issues. Computer modeling, though holding significant promise for creating alternative pediatric head surrogates, encounters numerous challenges because of the intricacies of child growth and development. A finite-element (FE) model of an infant head was created from high-resolution CT scans, utilizing published data on tissue material properties. Biofidelity was verified through comprehensive validation against existing PMHS data by simulating experimental impact tests, focusing on the infant head's kinematic response. This surrogate offers a valuable biomechanical engineering insight into how an infant's head behaves under impact loads, which will subsequently aid clinical and forensic management and injury prevention strategies.

Keywords: Biomechanics, Finite element modelling, Injury, Infant cranial trauma, Material characteristics, Post-mortem human surrogates

1. Introduction

Traumatic brain injury (TBI), resulting from a vehicle collision or fall, is the foremost cause of death and long-term disability from injury in children [1]. Finite element (FE) analysis has become an effective approach to studying head injury mechanics and assessing head injury risk. However, there is a scarcity of pediatric FE head models to predict the occurrence of skull fractures and neurological injuries, compared to the numerous FE adult head models [2–4]. The development of pediatric head FE models is hindered by the limited availability of material property data, quantitative age-specific anatomical data, and pediatric impact response data. Ideally, the biofidelity of an FE head model, subjected to impact loading, requires validation from impact response data obtained from experimental impact testing on PMHSs, although this data is also limited. To the authors' knowledge, the first documented use of an FE head model for examining head trauma in infants was a study on head deformations during childbirth, aimed at understanding mechanical cranial birth injuries, conducted by McPherson and Kriewall [5] in 1980. McPherson and Kriewall [5] created an FE model of the parietal bones of a fetal skull, using bone stiffness properties derived from material experiments on fetal parietal bone [6], to elucidate the biomechanics of fetal skull deformation during the birthing process and to delineate the differences in skull bone stiffness between preterm and term infants during head deformation. Lapeer and Prager in 2001 [7] expanded and refined the work of McPherson and Kriewall [5], employing FE analysis to comprehend head molding during natural childbirth. However, it was not until the study by Thibault and Margulies in 2000 [8] that FE analysis was used to assess impact-induced deformations. Their FE simulations [8] integrated tissue

Received 5 August 2024; accepted 18 October 2024.
Available online 10 November 2024

E-mail address: ghaidaame85@gmail.com (G. Abdulrahman Khalid).

https://doi.org/10.70645/3078-3437.1011

response data from previous experimental tests on infant human cranial bone and porcine bone suture samples [9], to investigate the protective effects of the infant cranium and sutures on the brain. In 2007, Roth et al. [10] published a study on an FE model of a 6-month-old head to evaluate its dynamic response during impact and shaking. Using this 6-month FE model as a baseline, Roth et al. [11] in 2008 examined the effects of scaling by comparing the original model with a 6-month model derived from scaling down an adult FE model. Model conformity was evaluated in terms of the precision of head geometry, shape, and thickness. In 2009, Roth et al. [12] conducted a similar geometric analysis of a scaled FE head model of a 3-year-old child to reconstruct accidental scenarios. Subsequently, there has been a rise in researchers investigating the use of FE analysis for infant head trauma. This trend can be attributed to the increasing availability of human infant skull material properties in literature [13], providing a more accurate depiction of material response. Additionally, it can be partly explained by the greater availability of software that converts radiological images into 3D computer models, which can then be exported into computer-aided design (CAD) formats such as stereolithography (STL) and subsequently meshed to run in FE solvers like Abaqus (Dassault Systèmes) or LS-Dyna (Livermore Software Corporation). This, combined with enhanced computational power, has enabled the improved construction and validation of pediatric FE head models against pediatric PMHS impact response data. Following Coats and Margulies' [13] quantification of the material properties of human infant bone and sutures, Coats et al. [14] developed an FE model of a 5-week-old infant head using CT and MRI scans with the incorporated material data. Additionally, several researchers have utilized FE head models to represent young children [10–12, 14, 15]. However, while these FE models offer insights into head injury mechanics, they are limited because their validity has not been evaluated against experimental pediatric PMHS data. Alongside the FE head models and experimental characterization of biological tissues, Prange et al. [16] investigated the global response of the entire pediatric PMHS head subjected to impact drop tests. Impact tests were conducted on the frontal, occipital, vertex, and parietal areas, and the impact forces were measured and accelerations calculated. Although the aforementioned pediatric FE head models provide valuable insights for studying child head injuries, only Roth et al. [17] and Li et al. [18] validated their models against PMHS test data from a similarly aged group. However, both [17] and [18] represented the material properties of the infant cranial bone as homogeneous and isotropic using average material properties from the literature, rather than the heterogeneous, anisotropic material properties reported by McPherson and Kriewall [6]. Since the cranial bones significantly contribute to the overall head impact response, accurately representing the material properties is crucial to achieve the highest degree of biofidelity. To address these modeling limitations, this current study advances the development of a biofidelic infant FE head model, validated against real-world PMHS impact tests. This was accomplished by creating: an accurate geometric representation of bones, sutures, and fontanelles from high-resolution CT scan slices, a mathematical approach to replicating the anisotropic properties of cranial bones, a simulation of the documented fiber orientation in immature cranial bone, a valid and compatible mesh model for effective application in a finite element analysis model, and a numerical simulation and validation against published PMHS infant head impact data [16]. This enhances the understanding of infant head impact response and injury mechanics.

2. Materials and methods

2.1. FE modelling approach of the complete head

The high-resolution CT dataset was imported into Mimics 3D Medical Image Processing software to create a detailed 3D model of an infant's skull. The skull was divided into four segments: parietal, occipital, frontal bones, and the skull base. Thresholding techniques were applied to distinguish between skeletal and soft tissue structures, supported by manual editing to address irregular areas. A soft tissue mask was segmented, and morphological closing was used to seal cavities. The cervical vertebrae and mandible were removed, and the bones were smoothed to improve the 3D CAD model's definition. The occipital bone was adjusted to align with the parietal bones for a more representative model as in Fig. 1.

Several attempts to separate the sutures from the cranial bones using standard tools were unsuccessful due to similar pixel greyscale values. Various tools, including wrapping and Boolean operations, were employed to achieve the final suture model. Shared borders were created between adjacent parts, and the 'non-manifold' tool was used to eliminate gaps and create a unified assembly for the 3D bone and soft tissue models. This method proved effective for the complex geometry of the pediatric head model, resulting in the final assembled model as in Fig. 2. After creating the 3D CAD head model, a valid and compatible mesh model was generated. The final 3D representation of the infant head was meshed using

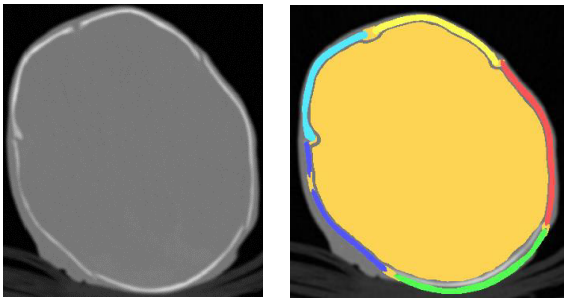

(a) (b)

Fig. 1. Sagittal aspect of the infant head with different structural greyscale values (a) outline of depressed occipital bone (b) occipital bone moved inline, contrast illustrating parts with different threshold values.

a second-order tetrahedral mesh in Mimics Remesh (3-matic v.10). This algorithm applied a smoothing function with a Laplacian first-order method (smoothing factor = 0.7), repeated 100 times for each part. Various quality parameters and element mesh sizes were used to optimize the mesh quality and reduce the number of elements, enhancing accuracy and reducing computational time. The 'fix wizard' analysis checked for faults like inverted "normals," bad edges, noise shells, and intersecting triangles. The 'quality preserving reduce triangles' (QPRT) algorithm was then applied, and the volume mesh was created. The mesh quality was inspected using the edge ratio, equivalent to the aspect ratio in Abaqus/Explicit. Finally, the model was exported to Abaqus/Explicit (v6.12) to simulate the kinematics of infant head impact as in Fig. 2.

2.2. Material properties

Previous efforts to create validated infant FE head models have treated cranial bone material properties as uniform and isotropic [10–12, 15, 17, 18]. However, pediatric cranial bone is thin, heterogeneous, and highly curved with a distinct fiber orientation [6]. At birth, these bones show a visible fiber pattern due to trabeculae radiating from ossification centers (Fig. 4a). McPherson & Kriewall [6] found differences in the elastic modulus between tangential and radial fiber orientations. Coats & Margulies [13] reported that infant cranial bone is inhomogeneous, with varying stiffness in parietal and occipital bones. These variations confirm the significant anisotropic nature of immature cranial bone. Consequently, the cranial bones in this FE model were modeled as in-plane orthotropic with different elastic moduli parallel and perpendicular to the fibres. The material constant for orthotropic material was calculated using a mathematical equation in Abaqus software [20].

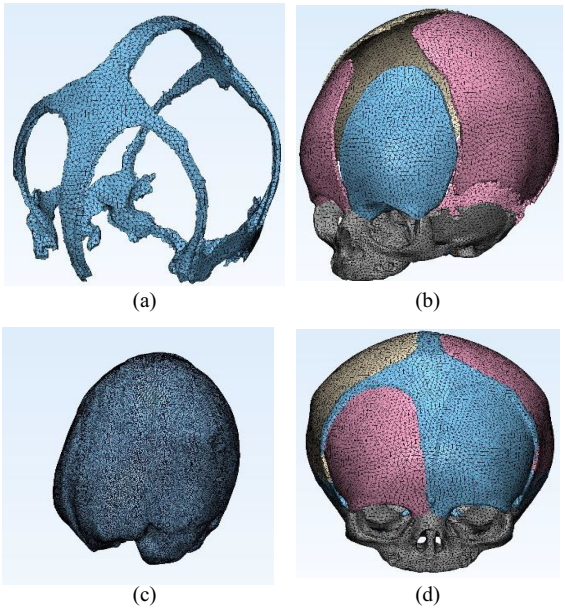

(a) (b) (c) (d)

Fig. 2. The structures of the infant's head (a) sutures (b) cranial bones (c) brain (d) complete structure of the head.

The constitutive equations of stress, represented as a vector, σ, as a function of the strain vector, ϵ, (with elasticity matrix E) used in this study are as follows:

$$\sigma = E\varepsilon \tag{1}$$

According to McPherson and Kriewall [6], the parietal bone stiffness ratio between parallel and perpendicular orientations is 4.2:1, and for the frontal bone, it is 1.8:1. No tests were conducted on occipital bones; therefore, a ratio of 4.2:1 was assumed, similar to the parietal bones. The infant cranial bones were modeled as an orthotropic solid element material in Abaqus (Version 6.12, DSS 12) and defined based on the elastic stiffness matrix [20] outlined in Eqs. (2)–(12) below:

$$\begin{Bmatrix} \sigma_{11} \\ \sigma_{22} \\ \sigma_{33} \\ \sigma_{12} \\ \sigma_{23} \\ \sigma_{22} \end{Bmatrix} = \begin{bmatrix} D_{1111} & D_{1122} & D_{1133} & 0 & 0 & 0 \\ 0 & D_{2222} & D_{2233} & 0 & 0 & 0 \\ 0 & 0 & D_{3333} & 0 & 0 & 0 \\ 0 & 0 & 0 & D_{1212} & 0 & 0 \\ 0 & 0 & 0 & 0 & D_{1313} & 0 \\ 0 & 0 & 0 & 0 & 0 & D_{2323} \end{bmatrix} \begin{Bmatrix} \varepsilon_{11} \\ \varepsilon_{22} \\ \varepsilon_{33} \\ \gamma_{12} \\ \gamma_{13} \\ \gamma_{23} \end{Bmatrix} \tag{2}$$

$$D_{1111} = E_1(1 - \nu_{23}\nu_{23})\Gamma \tag{3}$$

$$D_{2222} = E_2(1 - \nu_{13} - \nu_{31})\Gamma \tag{4}$$

$$D_{2233} = E_2(\nu_{32} - \nu_{12}\nu_{31})\Gamma \tag{5}$$

$$D_{1122} = E_1(\nu_{21} - \nu_{31}\nu_{23})\Gamma \tag{6}$$

$$D_{1133} = E_1(\nu_{31} - \nu_{21}\nu_{32})\Gamma \tag{7}$$

$$D_{2233} = E_2(\nu_{32} - \nu_{21}\nu_{31})\Gamma \quad (8)$$

$$D_{1212} = G_{12} \quad (9)$$

$$D_{1313} = G_{13} \quad (10)$$

$$D_{2323} = G_{23} \quad (11)$$

$$\Gamma = \frac{1}{(1 - \nu_{12}\nu_{21} - \nu_{23}\nu_{32} - \nu_{13}\nu_{31} - 2\nu_{21}\nu_{32}\nu_{13})} \quad (12)$$

The material constants used in the FE model were the elastic moduli, shear moduli, and Poisson's ratios (E1, E2, E3, G12, G23, ν12, ν23, ν13, E, G, ν), respectively; where subscript "1" refers to the parallel fiber direction, subscript "2" pertains to the perpendicular direction, and subscript "3" denotes the direction perpendicular to both 1 and 2. Only E2 is known for each cranial bone from high-rate material testing [13]. Therefore, E1 was calculated using the scaling method of McPherson and Kriewall [6]. It was assumed that E3 is equivalent to E2. Poisson's ratio (ν23) was assumed to be equivalent to the Poisson's ratio for tangential compression of adult cranial bone, as reported by McElhaney et al. [21]. It was assumed that E3 is equivalent to E2; thus, due to symmetry, ν32, ν31, and ν21 were equal to ν23. The shear modulus G was calculated from Eq. (13):

$$G_{23} = \frac{E_2}{2(1 + \nu_{23})} \quad (13)$$

The asymmetric Poisson's ratio was determined using Eq. (14):

$$\frac{\nu_{12}}{E_1} = \frac{\nu_{21}}{E_2} \quad (14)$$

For asymmetric planes, Huber's in-plane orthotropic Eq. (15) was employed to calculate the shear modulus.

$$G_{12} = \frac{\sqrt{E_1 E_2}}{2(1 + \sqrt{\nu_{12}\nu_{21}})} \quad (15)$$

The material constants for the infant basilar skull bones (the skull base) are not available in the literature. Consequently, since the skull base and frontal bones are combined in the model, the values for the frontal bone are applied to the combined 'frontal bone' group. The material orientation can be seen in Fig. 3. The infant cranial suture was modeled as linear elastic, assigning the coronal suture the average elastic modulus reported for infants aged 0–12 months, with no significant effect of donor age [13]. To the authors' knowledge, it is unclear whether the original source location influences the material response

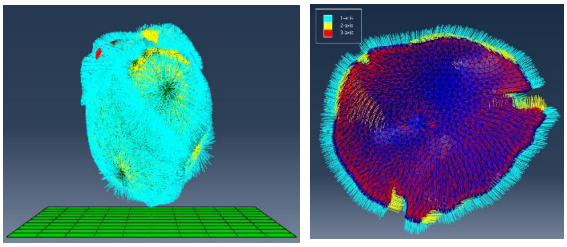

(a) (b)

Fig. 3. The anisotropic properties of (a) the complete structure of the head model and (b) cranial bone.

of the suture material. Thus, this value was used to represent all the infant sutures in the FE model. Furthermore, the density and Poisson's ratio of the suture are also unknown; therefore, it was assumed to be incompressible, with a density equal to that of the dura mater [21]. The material properties are listed in Table 1. The brain of the FE head model was modeled as isotropic and linear elastic. The gelatin material properties shown in Table 1 were assigned to the brain of the FE head model based on a previous study modeling the brain [22, 23].

2.3. Computational simulation

For nonlinear dynamic analyses, finite element solvers must use direct integration [20]. This method is less computationally intensive since a stiffness matrix is not needed at each time step. Although explicit analysis is limited by the smallest element size and the stress wave passage time, making the time steps small, it is well-suited for short-duration contact problems. Recognizing [10–12, 14, 15, 17, 18, 24–29], effectively used explicit solvers, explicit time integration was used for impact tests in this study. Abaqus used to study high-deformation impacts, with preliminary simulations. The longer simulations were run on High-Performance Computing. A mesh sensitivity analysis was operated to assess the impression of mesh resolution on convergence study output. The goal was to find the coarsest mesh that still produced accurate results. Reducing the mesh resolution below 20×10^5, while significantly decreasing computational running time, led to an increase in error. Consequently, a model with a resolution of 20×10^5 was used for the remaining analysis. It was chosen as the best mesh due to its comparatively least error and considerably shorter computational period. The ultimate head model mesh comprised 2,626,855 second-order adapted tetrahedral elements. The Post-Mortem-Human-Surrogate test [16] was used to validate the current head model by simulating the Prange et al. tests, as shown in Fig. 4. Different

Table 1. The material constant of the complete head model.

FE Head model structure	Material properties
Cranial bones	ρ =2.09E-09 tonne/mm3
Occipital	E1=1400 MPa, E2=333 MPa,E3=333 MPa ν12=0.19,ν13=0.045,ν23=0.22,ν21= 0.0451 G12=312 MPa,G13=312, MPa,G23=136.4 MPa
Parietal	E1=2300 MPa,E2=457 MPa,E3=457 MPa ν12=0.19,ν13=0.045,ν23=0.22,ν21= 0.0451 G12=513.3 MPa,G13=513.3 MPa,G23=244.1 MPa
Frontal	E1=2300 MPa,E2=1277 MPa,E3=1277 MPa ν12=0.19,ν13=0.11,ν23= 0.22,ν21= 0.1054 G12=750.6 MPa,G13=750.6 MPa,G23=523.3 MPa
Sutures and Fontanelles	ρ =1.13E-09 tonne/mm3 E= 8.1 MPa, ν =0.49
Brain	ρ =1.1 E-09 tonne/mm3,E= 0.0272 MPa ν =0.499

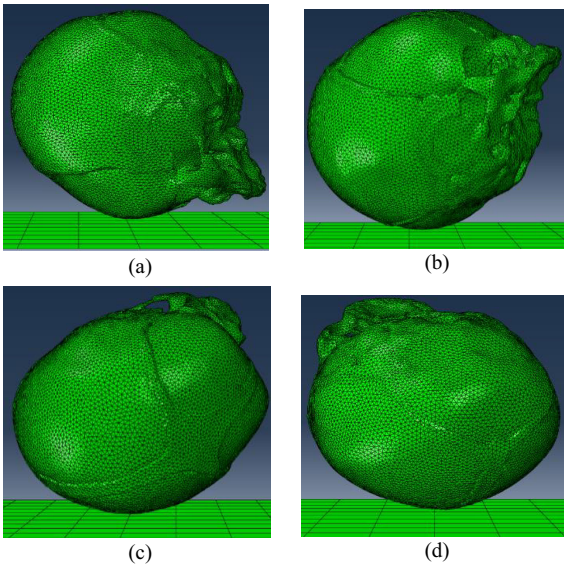

Fig. 4. The impact of the simulated head model onto a rigid surface at (a) Forehead region (b) Occiput region (c) Parietal region (d) Vertex region.

head impact states were implanted computationally and assessed against the impact response data from [16]. Through the eight impact simulations, the head model was positioned in interaction with the firm plane and allocated a pre-impact speed of 1.716 m/s or 2.426 m/s, consistent with impact heights (0.15 m or 0.30 m).

3. Results

The simulated head model was validated via a series of impact simulations aligned with the PMHS infant head impact experiments [16]. Impacts were simulated on different head regions (forehead, parietal, occipital, and vertex) from heights of 0.15 m and 0.3 m onto a rigid surface. Eight drop impact scenarios were included, corresponding to pre-impact velocities of 1.715 m/s and 2.425 m/s, respectively. Numerical acceleration was derived from the FE simulations by dividing the impact force by the head mass, similar to [16]. The mass of the current computational head model of a 10-day-old infant closely matched the mass of a 3-day-old infant PMHS head [16]. All peak acceleration values measured in this study are absolute and do not account for variation. Therefore, statistical significance cannot be evaluated for these parameters. However, a change greater than 15% between the FE model and PMHS tests [16] was noted, as used by previous authors [14, 17]. Validation involved comparing the numerical simulation of the current FE head model with the experimental results from the PMHS tests [16]. The results, shown in Fig. 5a-d, profile the acceleration–time impact response from a 0.30 m free fall onto four different head impact locations. Fig. 5a-d and Fig. 6 indicate that the peak resultant acceleration values for all eight drop tests correlate well under all conditions, with slight variances at the occipital, forehead, and parietal regions at both 0.15 m and 0.30 m, where the average peak accelerations of the FE model increased by more than 15% for the occipital, forehead, and parietal regions and less than 15% for the vertex impact at both 0.15 m and 0.30 m. A comparison of the output variables between this new FE head model and those in [16] can be seen in Fig. 6. The average peak accelerations of the occipital bone at both 0.15 m and 0.30 m for the FE model were 62.6 g and 101 g, respectively, exceeding the 46.0 g and 72.1 g for the PMHS response from the same height. The forehead responses were 77.8 g and 120.8 g for the FE head model, surpassing the PMHS test values [16] of 49.5 g and 82.1 g, respectively. The parietal responses were 67 g and 91.7 g for the FE

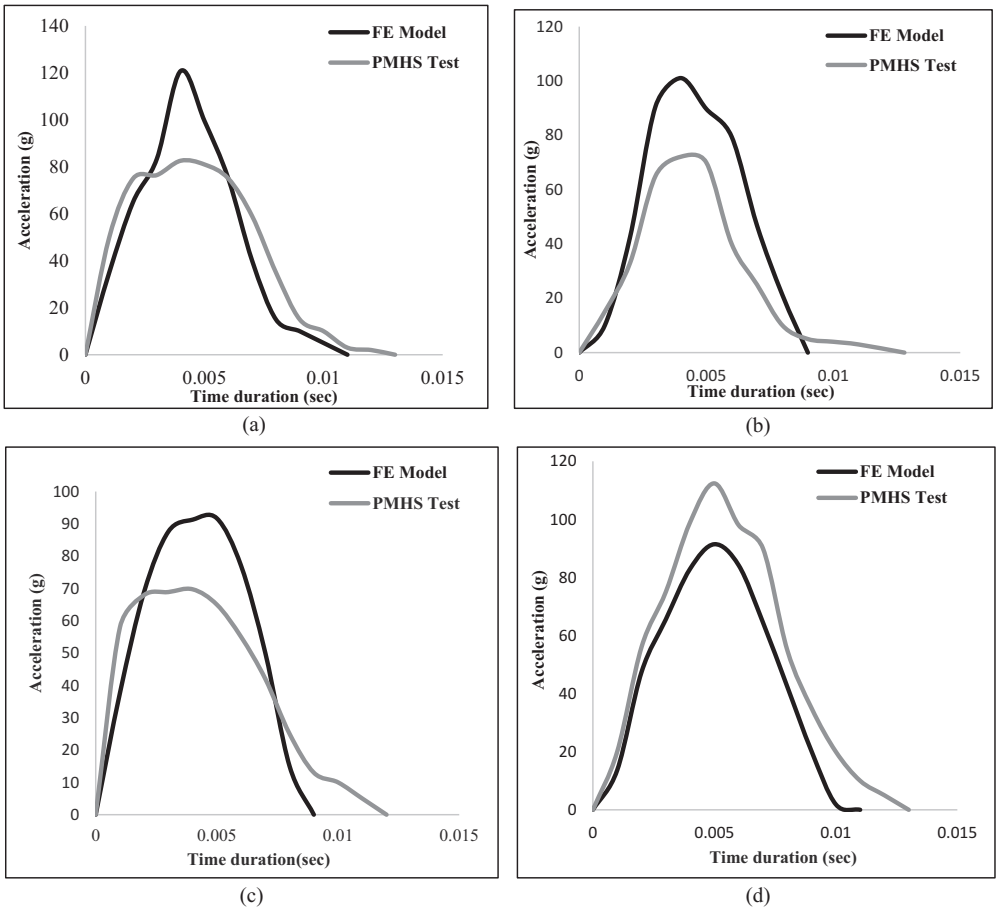

Fig. 5. The impact of the simulated model onto a rigid surface at the (a) forehead region (b) occiput region (c) parietal region (d) vertex region.

head model (acceleration >15%), compared to 44.5 g and 69.75 g in the PMHS tests [16]. For the vertex impact, all peak accelerations at both drop heights (0.15 m and 0.30 m) were less than 15% compared to the PMHS test [16]. Fig. 7 illustrates typical impact time durations between the PMHS tests and the FE model throughout the validation process. The average impact time durations for the FE model at both drop heights (0.15 m and 0.30 m) were observed to be slightly shorter than those in the PMHS tests [16]. Fig. 6 shows that the peak accelerations for the FE model were similar to the PMHS impact responses. However, the impact-time durations from the simulation were slightly shorter than those in the PMHS tests. Fig. 5a-d displays the acceleration-time contact curve of the forehead region at the 0.3 m drop height, demonstrating a slight variation in impact duration. Overall, the comparisons indicate that the pediatric FE head model responses are generally in good agreement with the PMHS results [16]. While some resultant peak acceleration values varied with different drop heights, they did not significantly differ across different impact locations.

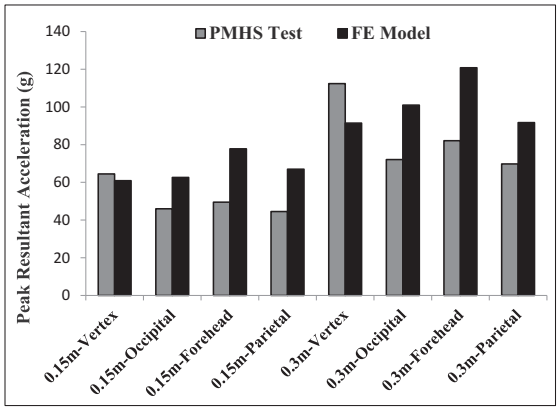

Fig. 6. The Peak resultant acceleration is established with different drop heights for head model impact tests.

4. Discussion

Paediatric Head Model Validation Regarding child head models, most current knowledge about paediatric head collision is built on the sole published quantitative PMHS experimental study by Prange

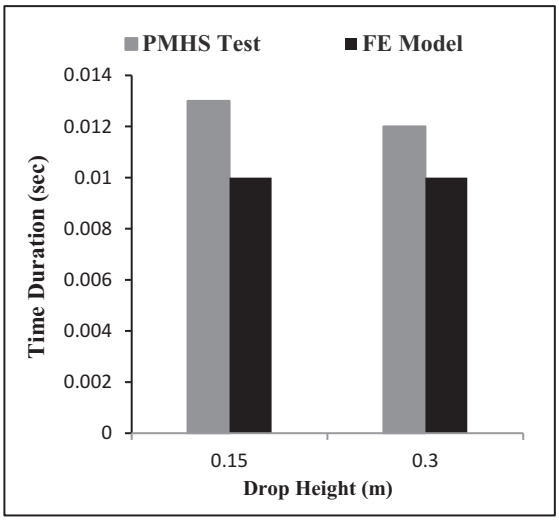

Fig. 7. The time at the point of head model impact is constructed on two different heights.

et al. [16], providing information on the overall behavior in terms of the acceleration-time response from different impact circumstances. During the head impact test, the acceleration response appeared to increase and decrease, as depicted by the acceleration-time waveform shown in Figs. 5a-d. In the early fragment of the appeared waveform, 'the increase,' the simualted model undergoes compressive deformation while decelerating. During the subsequent portion, the waveform peaks and plateaus due to the frequency change of model velocity among deceleration and acceleration. In the final portion, the profile reflects the restoration of the impact and touching surfaces jumping backwards to their pre-impact form, demonstrated through the model rebounding and accelerating off the surface.

Furthermore, from the numerical FE and experimental PMHS 0.3 m impacts, the acceleration-time responses shown in Fig. 5 exhibit a slight difference in pulse durations, providing information regarding the surface's ability to absorb impact energy. Since the impact surface affects the absorption of kinetic energy, acceleration response, and impact duration. From Fig. 5, the higher peak acceleration of the FE head model indicates that a 'rigid surface' offers little cushioning during impact, causing the FE model to decelerate over a short duration. During the PMHS tests, there were relatively lower peak accelerations due to the physical steel impact surface cushioning the impact, allowing the head to decelerate over a longer period while absorbing more impact energy. The contact time duration of the simulated model was slightly larger than the PMHS, as shown in Fig. 7, for both the 0.15 m and 0.3 m drop heights.

It is noteworthy that, unlike the decision to align the occipital bone with the parietal bones in this study, the PMHS experiments [16] were conducted on three newborn specimens (ages 1, 3, and 11 days old), so it is entirely possible that the heads had depressed occipital bones. Simulated FEA of head impacts were performed with different head orientations, as shown in Fig. 4. Figs. 5b and 6 indicate that higher accelerations were produced during the FE simulation compared to the PMHS experiments [16]. Across the simulated tests of the parietal region (shown in Fig. 4c), it appeared both the occipital bone position plus the impact site (see Figs. 1b, and 4c) seem to influence the response of the model parietal bone. Since assumed above, an inline head occipital bone comparative to the parietal bone is expected to generate larger acceleration rates, possibly as a result of a further "shell-like" formation. Related to the vertex region of impacts as in Fig. 4d, the simulated model response (see Figs. 5d and 6) was very close to the PMHS study [16] by fall heights of 0.15 m and 0.3 m. In imitation of loading the parietal region, the model seems stiffer near the posterior section. Additionally, while the target was to force the parietal region at its center, the impact force was monitored to be considerably near the posterior zone of the parietal cranial bone, because of its irregular form. Later, this, by the inline occipital cranial bone, might clarify the greater acceleration exposed in Figs. 5c and 7.

Regarding the forehead drop test in Fig. 4a, presents a difference in the impact output between the simulated model and the Post-Mortem-Human-Surrogate experiment as outlined in Fig. 7. The simulated head model forehead responses were 77.8 g and 120.8 g, compared to the PMHS test results of 49.5 g and 82.1 g, at 0.15 m and 0.30 m, respectively. Variations could be due to differences in sites of impact between the simulated model and the Post-Mortem-Human-Surrogate experiments. Anatomically, the inferior section of the model forehead which fairly stiff, since it consists of numerous compound structures. Resulting in reasonably high accelerations while impacting this region. Compared to the impact that take place at the forehead upper section, near the lenient bone and fontanelle, a lower response could be believed. For both the PMHS experiments and FE simulation, a rigid body assumption was made to calculate the impact acceleration by dividing the impact force by the head mass. While this approach is valid for rigid entities such as anthropometric test device (ATD) dummy heads, it is a limitation for pediatric head models, as they are more flexible and have more deformable structures. Therefore, no acceleration could be evaluated at the center of gravity for validation purposes. The

suitability of the rigid body approximation for investigating head injury risk is the subject of current and future investigations [30–41]. It is noteworthy that while, the peak accelerations for most impact locations are slightly greater in the simulated model than the the Post-Mortem-Human-Surrogate impact response, the values still fall within Prange's [16] published PMHS impact response corridors. The current approach of linking high-resolution scans with modelling of infant material response data, validated against PMHS impact response data, with minimal computational time, has proven to be an important step in characterizing and identifying pediatric head injury mechanisms [36, 38, 40]. While overcoming many shortcomings of pediatric head impact biomechanical studies, which rely on a global approximation of head response rather than the present localized kinematic metrics arising from the complex pediatric head anatomy and heterogeneous and anisotropic mechanical properties of head materials [36, 38] this approach provides a valuable biomechanical representation of how an infant's head reacts through impact [32, 34, 37, 41].

5. Conclusions

Infant Post Mortem Human Surrogate (PMHS) experimentation, a rational method for understanding injury biomechanics, is severely restricted, largely due to the scarcity of surrogates, a consequence of emotional, moral, and ethical considerations. To address this limitation, this study developed a biofidelic infant FE head model from high-resolution computed tomography (CT) scans, informed by published tissue material properties, to simulate and investigate infant fall-related head impacts. Infant head modeling presents many unique challenges due to the complexities of child growth and development, resulting in age-dependent changes in anatomy, geometry, and physical response characteristics. Moreover, unique to infants, cranial bones exhibit greater flexibility than adult bones and a visible bone fiber orientation due to trabeculae radiating from growth centers, which are radially orthotropic. To replicate the fiber orientation of immature cranial bone, radially orthotropic properties were applied to an FE cranial bone model, with elastic moduli representing the bone response both parallel and perpendicular to the fiber orientation. Additionally, since infant cranial bones are also separated by relatively flexible sutures and fontanelles, appropriate tissue response properties were also modeled. The biofidelity of the computational model was confirmed by global validation against published PMHS data by replicating experimental impact tests with a series of computational simulations in terms of the infant head's kinematic response. In comparison to the pediatric (PMHS) test data, the kinematic impact response of the FE head model showed a good agreement with those from the PMHS drop test data. The current FE head surrogate provides a valuable biomechanical engineering insight into how an infant's head responds during impact loading, which is expected to notify the medical and scientific organization besides injury prevention policies.

References

1. L. Trefan, R. Houston, G. Pearson, R. Edwards, P. Hyde, I. Maconochie, R. Parslow, and A. Kemp, "Epidemiology of children with head injury: A National Overview," *Arch. Dis. Child.*, vol. 101, no. 6, pp. 527–532, 2016.
2. A. Nahum, R. Smith, and C. Ward, "Intracranial pressure dynamics during head impact," Proceedings of the 21st STAPP Car Crash Conference. pp. 339–366. 1977.
3. W. Hardy, C. Foster, M. Mason, K. Yang, A. King, and S. Tashman, "Investigation of head injury mechanisms using neutral density technology and high-speed biplanar X-ray," *Stapp. Car Crash J.*, vol. 45, pp. 337–368, 2001.
4. N. Yoganandan, F. Pintar, A. Sances, P. Walsh, C. Ewing, T. Snyder, and R. Snyder, "Biomechanics of skull fracture," in: Proceedings of the Head Injury Symposium,Washington, DC, pp. 227–236. 1994.
5. G. McPherson and T. Kriewall, "Fetal head molding: An investigation utilizing a finite element model of the foetal parietal bone," *J. Biomech.*, vol. 13, no. 1, pp. 17–26, 1980.
6. G. McPherson and T. Kriewall, "The elastic modulus of foetal cranial bone: a first step towards an understanding of the biomechanics of foetal head molding," *J. Biomech.*, vol. 13, no. 1, pp. 9–16, 1980.
7. R. Lapeer and R. Prager, "Fetal head moulding: finite element analysis of a fetal skull subjected to uterine pressures during the first stage of labour," *J. Biomech.*, vol. 34, no. 9, pp. 1125–1133, 2001.
8. K. Thibault and S. Margulies, "Age-dependent material properties of the porcine cerebrum: effect on pediatric inertial head injury criteria," *J. Biomech.*, vol. 31, no. 12, pp. 1119–1126, 1998.
9. S. Margulies and K. Thibault, "Infant skull and suture properties: measurements and implications for mechanisms of pediatric brain injury," *J. Biomech. Eng.*, vol. 122, p. 364, 2000.
10. S. Roth, J.-S. Raul, B. Ludes, and R. Willinger, "Finite element analysis of impact and shaking inflicted to a child," *Int. J. Legal Med.*, vol. 121, no. 3, pp. 223–228, 2007.
11. S. Roth, J. Raul, and R. Willinger, "Biofidelic child head FE model to simulate real world trauma," *Comput. Methods Programs Biomed.*, vol. 90, no. 3, pp. 262–274, 2008.
12. S. Roth, J. Vappou, J. Raul, and R. Willinger, "Child head injury criteria investigation through numerical simulation of real world trauma," *Comput. Methods Programs Biomed.*, vol. 93, no. 1, pp. 32–45, 2009.
13. B. Coats and S. Margulies, "Material properties of human infant skull and suture at high rates," *J. Neurotrauma*, vol. 23, no. 8, pp. 1222–1232, 2006.

14. B. Coats, S. Ji, and S. Margulies, “Parametric study of head impact in the infant,” *Stapp. Car Crash J.*, vol. 51, pp. 1–15, 2007.
15. S. Roth, J. Raul, J. Ruan, and R. Willinger, “Limitation of scaling methods in child head finite element modelling,” *Int. J. Veh. Saf.*, vol. 2, no. 4, pp. 404–421, 2007.
16. M. Prange, J. Luck, A. Dibb, C. Van Ee, R. Nightingale, and B. Myers, “Mechanical properties and anthropometry of the human infant head,” *Stapp. Car Crash J.*, vol. 48, p. 279, 2004.
17. S. Roth, J. S. Raul, and R. Willinger, “Finite element modelling of pediatric head impact: Global validation against experimental data,” *Comput. Methods Programs Biomed.*, vol. 99, no. 1, pp. 25–33, 2010.
18. Z. Li, J. Hu, M. P. Reed, J. Rupp, C. Hoff, J. Zhang, and B. Cheng, “Development, validation, and application of a parametric pediatric head finite element model for impact simulations,” *Ann. Biomed. Eng.*, vol. 39, no. 12, pp. 2984–2997, 2011.
19. A. Juke, D. Baird, D. Weinberg, D. McConnaughey, and A. Wilcox, “Length of human pregnancy and contributors to its natural variation,” *Hum. Reprod.*, vol. 28, no. 10, pp. 2848–2855, 2013.
20. Abaqus User’s Manual. Dassault Systemes 2010.
21. J. Galford and J. McElhaney, “A viscoelastic study of scalp, brain, and dura,” *J. Biomech.*, vol. 3, no. 2, pp. 211–221, 1970.
22. J. Crandall, B. Myers, D. Meaney, and S. Zellers Schmidtke, Pediatric Injury Biomechanics. 1st ed. New York, NY: Springer, 2013.
23. J. Cheng, I. Howard, and M. Rennison, “Study of an infant brain subjected to periodic motion via a custom experimental apparatus design and finite element modelling,” *J. Biomech.*, vol. 43, no. 15, pp. 2887–2896, 2010.
24. G. Khalid and M. Jones, “Preliminary Numerical Simulations to Investigate the kinematics of Infant Head Impact,” Proceedings of the 24th UK Conference of the Association for Computational Mechanics in Engineering, Cardiff University, Cardiff, 2016.
25. G. Khalid, M. Jones, R. Prabhu, A. Mason-Jones, W. Whittington, and P. Theobald, “Development of paediatric head models for the computational analysis of head impact interactions,” 19th International Conference on Computational Modeling, Analysis and Simulation, London, UK, 2017.
26. K. Klinich, G. Hulbert, and L. Schneider, “Estimating infant head injury criteria and impact response using crash reconstruction and finite element modelling,” *Stapp. Car Crash J.*, vol. 46, p. 165, 2002.
27. Z. Li, X. Luo, and J. Zhang, “Development/global validation of a 6-month-old paediatric head finite element model and application in investigation of drop-induced infant head injury,” *Comput. Methods Programs Biomed.*, vol. 112, no. 3, pp. 309–319, 2013.
28. S. Ji and S. S. Margulies, “In vivo pons motion within the skull,” *J. Biomech.*, vol. 40, no. 1, pp. 92–99, 2007.
29. R. Miller, S. Margulies, M. Leoni, M. Nonaka, X. Chen, D. Smith, and D. Meaney Finite Element Modeling Approaches Of Predicting Injury In An Experimental Model Of Severe Diffuse Axonal Injury. 1998. Report No.: 0768002931.
30. G. A. Khalid, “Density and Mechanical Properties of Selective Silicon Materials to Produce 3D Printed Paediatric Brain Model,” *MSF*, vol. 1021, pp. 220–230, 2021, doi: https://doi.org/10.4028/www.scientific.net/msf.1021.220.
31. M. D. Jones, G. A. Khalid, and R. K. Prabhu, “Development of a Coupled Physical–Computational Methodology for the Investigation of Infant Head Injury,” *Multiscale Biomechanical Modeling of the Brain*, pp. 177–192, 2022.
32. G. A. Khalid et al., “Preliminary Numerical Simulations to Investigate the Kinematics of Infant Head Impact,” In Proceedings of the 24th UK Conference of the Association for Computational Mechanics in Engineering, 2016.
33. A. J. Al-Graitti, G. A. Khalid, P. R. Berthelson, R. K. Prabhu, and M. D. Jones, “A Comparative Study of the Kinematic Response and Injury Metrics Associated with Adults and Children Impacted by an Auto Rickshaw,” In: K. Arai, R. Bhatia, S. Kapoor (eds) Intelligent Computing. CompCom 2019, Advances in Intelligent Systems and Computing, vol 997. Springer, Cham, 2019, https://doi.org/10.1007/978-3-030-22871-2_29.
34. G. A. Khalid, R. Prabhu, J. Dickson et al., “Biomechanical Engineering Investigation of the Risk of Children Wearing a Bicycle Helmet Suffering an Angular Acceleration Induced Head Injury,” *MOJ Sports Med.*, vol. 1, no. 5, pp. 109–115, 2017, doi: 10.15406/mojsm.2017.01.00025.
35. G. A. Khalid, M. D. Jones, R. Prabhu, A. Mason-Jones, W. Whittington, H. Bakhtiarydavijani, and P. S. Theobald, “Development of a Paediatric Head Model for the Computational Analysis ofHead Impact Interactions,” *Int. J. Math. Comput. Phys., Electr. Comput. Eng.*, vol. 4, no. 3, pp. 113–116, 2017.
36. G. A. Khalid, “ A Coupled Physical – Computational Methodology for the Investigation of Short Fall Related Infant Head Impact,” PhD Thesis, Cardiff University, 2018.
37. A. Bakhtiarydavijani, G. Khalid, M. Murphy, K. Johnson, L. Peterson, M. Jones, M. Horstemeyer, A. Dobbins, and R. Prabhu, “A Mesoscale Finite Element Modelling Approach for Understanding Brain Morphology and Material Heterogeneity Effects in Chronic Traumatic Encephalopathy,” *Comput. Methods Biomech. Biomed. Eng.*, vol. 24, no. 11, pp. 1169–1183, 2020.
38. G. A. Khalid, R. K. Prabhu, O. Arthurs, and M. D. Jones, “A Coupled Physical-Computational Methodology for the Investigation of Shortfall Related Infant Head Impact Injury,” *Forensic Sci. Int.*, vol. 300, pp. 170–186, 2019, doi: https://doi.org/10.1016/j.forsciint.2019.04.034.
39. G. A. Khalid, H. Bakhtiarydavijani, W. R. Whittington, R. Prabhu, and M. D. Jones, “Material Response Characterization of Three Poly Jet Printed Materials Used in a High Fidelity Human Infant Skull,” *Mater. Today: Proc.*, vol. 20, Part 4, pp. 408–413, 2020, doi: https://doi.org/10.1016/j.matpr.2019.09.156.
40. M. Jones, D. Darwall, G. Khalid, R. Prabhu, A. Kemp, O. J. Arthurs, and P. Theobald, “Development and Validation of a Physical Model to Investigate the Biomechanics of Infant Head Impact,” *Forensic Sci. Int.*, vol. 276, pp. 111–119, 2017, doi: https://doi.org/10.1016/j.forsciint.2017.03.025.
41. G. A. Khalid, “Biomechanical Investigation of the Efficacy of Conventional Bicycle Helmets at Preventing Facial Injury,” *J. Tech.*, vol. 4, no. 4, pp. 95–104, 2022, doi: https://doi.org/10.51173/jt.v4i4.867.